ADVANCED HEALTHCARE MATERIALS
www.advhealthmat.de

Rod-shaped Polymerized Salicylic Acid Particles Modulate Neutrophil Transendothelial Migration in Acute Inflammation

*M. Valentina Guevara, Emma R. Brannon, Daniel Kupor, Mariana R.N. Lima, Logan D. Piegols, Michael L. Felder, Kathryn E. Uhrich, and Omolola Eniola-Adefeso**

Neutrophilic inflammation is present in numerous high-mortality pathologies, including sepsis, deep vein thrombosis, and acute lung injury (ALI). Therefore, regulating neutrophil recruitment becomes an attractive therapeutic approach for neutrophil-mediated inflammation. Here, the impact of salicylic acid-based polymeric particles in regulating neutrophil recruitment in vivo and in vitro, particularly investigating the impact of neutrophil targeting via particle geometry-driven phagocytosis is explored. It is found that rod-shaped polymeric particles can improve neutrophil targeting in a murine ALI model, effectively preventing neutrophil infiltration into the mice's lungs compared to spherical particles of the same volume. It is demonstrated that the elongated nature of the polymeric carriers reduced neutrophils' transmigration ability across endothelial barriers in vivo and in vitro, contributing to their therapeutic effectiveness. These data represent initial work in developing non-spherical particle-mediated targeting of activated neutrophils for conditions affected by neutrophilic injury.

1. Introduction

Neutrophils constitute 50–70% of humans' circulating white blood cell population. Although neutrophils are short-lived cells, they play a fundamental, first-responder role in inflammation.[1,2] In a pathogenic invasion or injury, neutrophils are captured from circulation upon sensing inflammatory stimuli and adhere to the inflamed endothelium due to the binding interaction of neutrophil-endothelial cell ligands, leading to their rapid exit from the bloodstream.[1,3] Once neutrophils have trafficked through the vascular barrier, they exert different effector functions to manage and contain inflammation, including eliminating invading pathogens through phagocytosis, the release of granules, and the secretion of neutrophil extracellular traps (NETs) to entrap and kill microorganisms.[1,4,5]

While neutrophilic action is an essential aspect of the innate immune response, activated neutrophils can also amplify their recruitment and effector functions, leading to uncontrolled accumulation of neutrophils and tissue injury at the inflamed sites.[1,2] Indeed, unrestricted neutrophil function is present in the pathogenesis of a wide variety of diseases, including acute respiratory distress syndrome (ARDS),[6] sepsis,[7] ischemic stroke,[8] and vascular thrombosis.[9,10] Therefore, research efforts have explored restraining the innate neutrophil response to control neutrophil-mediated tissue damage. However, these potential approaches have had limited outcomes due to the complexity and heterogeneity of each condition.[1] For example, pharmacological treatment with sivelestat, a neutrophil elastase inhibitor used to manage pulmonary inflammation in ARDS, has shown limited or mixed clinical efficacy.[11–13] Similarly, anti-adhesive therapies interfering with leukocyte recruitment have failed to show clinical benefits in multiple neutrophil-driven pathologies in humans.[14–16]

Alternatively, recent work has explored targeting leukocytes with particulate drug carriers to modulate infiltrating immune cells' functions.[2,17] Specifically, researchers have implemented particles to inhibit neutrophils' interaction with the endothelium to control neutrophil accumulation in acutely inflamed areas and prevent further organ damage.[18–26] For instance, prior work reported that the internalization of piceatannol-loaded albumin nanoparticles by activated neutrophils reduced the number of adherent cells to inflamed venules and prevented leukocyte transmigration.[21] Similarly, some recent studies have revealed that the phagocytosis of cargo-free polymeric carriers by

M. V. Guevara, E. R. Brannon, D. Kupor, L. D. Piegols, M. L. Felder, O. Eniola-Adefeso
Department of Chemical Engineering
University of Michigan
Ann Arbor, MI 48109, USA
E-mail: lolaa@umich.edu
M. R. Lima, K. E. Uhrich
Department of Chemistry
University of California
Riverside, Riverside, CA 92521, USA
O. Eniola-Adefeso
Department of Biomedical Engineering
University of Michigan
Ann Arbor, MI 48109, USA

The ORCID identification number(s) for the author(s) of this article can be found under https://doi.org/10.1002/adhm.202404955

DOI: 10.1002/adhm.202404955

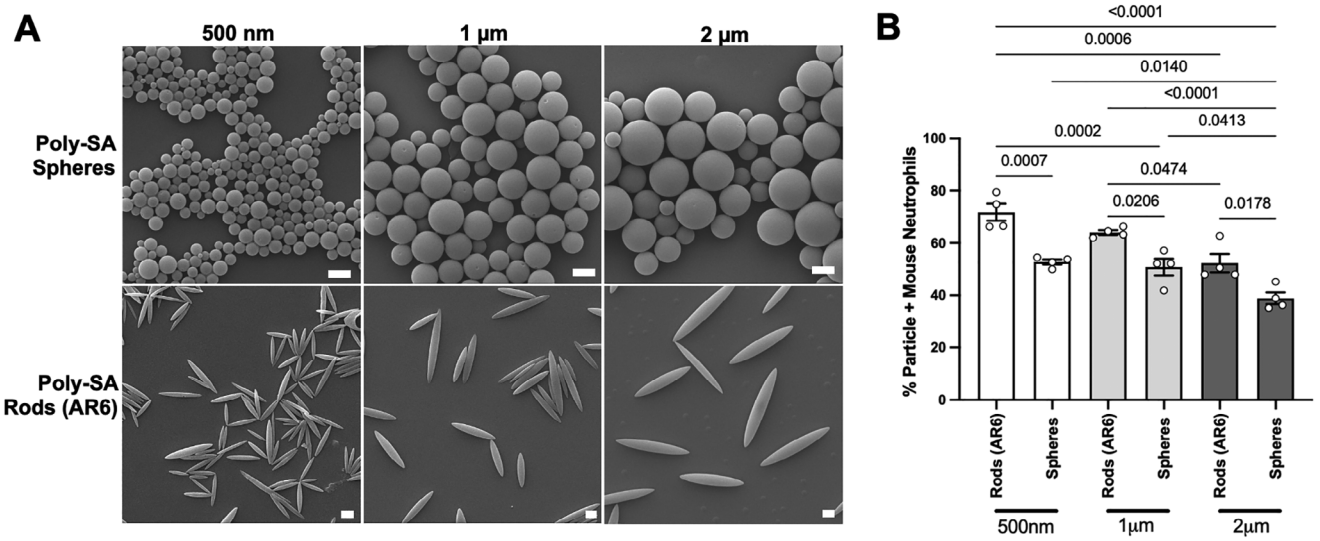

Figure 1. Ex vivo uptake of Poly-SA spheres and AR6 rods by mouse neutrophils. A) Scanning electron microscopy (SEM) images of 500 nm, 1 µm, and 2 µm spheres of Poly-SA polymer and the derived AR6 rods fabricated via a heat stretching technique. Scale bars (white bars) are 1 µm for spheres and rods. B) The percentage of mouse neutrophils that uptake rhodamine-labeled Poly-SA spheres and AR6 rods of equivalent spherical diameters of 500 nm, 1 µm, and 2 µm. Mouse blood was obtained via cardiac puncture, and particle concentration was set to 10^7 particles mL^{-1} of pooled whole mouse blood for all particle types and sizes. Statistical analysis was performed using One-way analysis of variance (ANOVA) with Tukey's post-test and 95% confidence interval for (B). The lack of symbols/values indicates no statistical significance. Circles in (B) represent individual pooled mouse blood samples treated with particles ($n = 4$).

activated neutrophils can also restrict leukocyte trafficking to inflamed areas and demonstrated that particles' therapeutic benefits go beyond the loaded drug content.[18,19,22,23] Notably, all the approaches mentioned above relied on neutrophil particle phagocytosis to lessen the inflammatory response.

Recent work by Safari et al. studied the ability of primary human neutrophils to internalize elongated polymeric particles. Contrary to other phagocytes like macrophages and monocytes, neutrophils displayed increased internalization of rod-shaped particles compared to spherical carriers of equal volume.[27] This departure from the literature inspired us to investigate the impact of elongated particles on targeting neutrophils via phagocytosis mechanisms. Thus, we hypothesized that rod-shaped particles could serve as particulate carriers to improve activated neutrophil targeting in acute inflammation.

To test this hypothesis, we fabricated cargo-free, anti-inflammatory, and biodegradable salicylic acid-based (Poly-SA) polymeric particles. Poly-SA polymer is a salicylate-derived poly(anhydride-esters) polymer designed for the controlled release of salicylic acid.[28,29] Salicylic acid exerts anti-inflammatory properties by inhibiting cyclooxygenase-2 transcription, thereby decreasing the formation of pro-inflammatory prostaglandins.[30,31] Recently, particulate carriers fabricated with Poly-SA polymer have been shown to modulate neutrophils' inflammatory response after particle phagocytosis. Poly-SA particles have effectively blocked neutrophil transmigration in a bacterial mouse model of ARDS,[19] decreased neutrophil-platelet aggregate adhesion in a murine model of thromboinflammation,[22] and reduced the progression and formation of NETs.[32] In this work, we fabricated Poly-SA spherical particles of 500 nm, 1 µm, and 2 µm size and heat-stretched them to form elongated Poly-SA particles of aspect ratio (AR) 6. Using a murine acute lung injury (ALI) model, we compared the ability of Poly-SA rods and spheres to modulate neutrophil transmigration to inflammation sites. We observed differences in the efficacy of blocking neutrophil infiltration based on particle shape. Furthermore, we demonstrated that the transmigration ability of particle-loaded neutrophils across an inflamed endothelial barrier can be prevented based on the carriers' shape.

2. Results

2.1. Mouse and Human Neutrophils Readily Phagocytose Poly-SA Spheres and Rods of Various Sizes

Prior studies reported that neutrophils can phagocytose rod-shaped polymeric particles more efficiently than spheres of equal volume, and the uptake of these rod-shaped particles improves with an increase in AR (AR $\geq$ 5).[26,27] Thus, we first confirmed mouse neutrophil uptake of high AR Poly-SA rods and Poly-SA spheres. Using a previously described film stretching technique, we utilized 500 nm, 1 µm, and 2 µm Poly-SA spheres to fabricate AR 6 rod-shaped Poly-SA particles (**Figure 1A**).[27,33] The major and minor axes for each Poly-SA rod type are listed in Table S1 (Supporting Information).

We obtained fresh pooled mouse blood via cardiac puncture from at least five healthy BALB/c mice and incubated the mouse blood with rhodamine-labeled Poly-SA spheres or rods for 2 h at 37 °C and 5% CO_2. We identified mouse neutrophils using flow cytometry as $CD11b^+Ly6G^+$ cells and further distinguished them with light-scattered plots and detected particle-positive mouse neutrophils by the positive signal for rhodamine (Figure S1, Supporting Information). We found that the percentage of mouse neutrophils internalizing 500 nm, 1 µm, and 2 µm Poly-SA AR

6 rods was significantly higher than neutrophils that phagocytosed spheres of equivalent volume (Figure 1B). Specifically, the association of mouse neutrophils with 500 nm Poly-SA rods increased by 36% relative to 500 nm spheres. Similarly, 1 μm and 2 μm Poly-SA rods showed a 26% and 35% increase in particle internalization compared to their respective spheres.

We also observed that mouse neutrophils were generally more associated with 500 nm and 1 μm Poly-SA rods and spheres than the 2 μm particles, as indicated by the higher percentage of particle-positive cells (Figure 1B). The 500 nm result was particularly appealing because nanoparticles pose a lower risk of causing occlusion in smaller capillaries.[2] Therefore, we investigated the therapeutic potential of nano-sized Poly-SA carriers since only micro-sized carriers have been used previously.[19,22,32] Prior work demonstrated that releasing salicylic acid from Poly-SA microparticles inside the cell helps tame neutrophil activation during inflammation.[19,32] However, it is unclear whether 500 nm Poly-SA nanoparticles would have a similar effect given their smaller polymer matrix and lower salicylic acid content than micron-sized particles (Figure S2, Supporting Information). Thus, we investigated CD62L shedding, a hallmark of neutrophil activation, on 500 nm particle-positive human neutrophils after lipopolysaccharides (LPS) exposure.[2,34] Unlike the micron-sized Poly-SA particles, 500 nm Poly-SA rods and spheres did not prevent CD62L shedding on particle-positive neutrophils after LPS exposure (Figure S3, Supporting Information). Due to the lack of anti-inflammatory activity of 500 nm Poly-SA carriers on activated neutrophils, we moved forward evaluating the 1 μm Poly-SA rod particles in further in vivo experiments, given their similar uptake rate with 500 nm rods.

Next, we evaluated the competitive uptake of the 1 μm Poly-SA rods and spheres by mouse monocytes in mouse blood. We identified mouse monocytes as $CD11b^{+}Ly6G^{-}Ly6C^{+}$ and determined particle-positive mouse monocytes by detecting the positive signal of rhodamine (Figure S4, Supporting Information). Similar to previous studies, we observed minimal differences in how monocytes in mouse blood phagocytose Poly-SA spheres versus rods (Figure S5, Supporting Information), in contrast to the particle uptake seen in mouse neutrophils (Figure 1B). Thus, our results show that mouse neutrophils exhibited a 4.6-fold increase in phagocytosis of elongated carriers when compared to the rod-shaped particles phagocytosed by mouse monocytes.

We also evaluated the internalization of Poly-SA particles by primary human neutrophils. We identified human neutrophils using flow cytometry using $CD11b^{+}$ cells, made further distinctions using forward-scatter and side-scatter panels, and determined particle-positive human neutrophils by the positive signal for rhodamine (Figure S6A, Supporting Information). We found that human neutrophils exhibited equivalent particle association with Poly-SA spheres and rods of each size (Figure S6B, Supporting Information). To investigate whether the observed equal level of phagocytosis was due to particle internalization being maximized at the timescale chosen (i.e., 2 h), we then evaluated the rate of Poly-SA particle uptake in human blood. We incubated whole human blood with 1 μm Poly-SA spheres and rods and recorded the percentage of particle-positive neutrophils at 15, 30, 60, and 120 min after particle addition. Surprisingly, primary human neutrophils phagocytosed 1 μm Poly-SA rods and spheres at the same rate, with no significant differences observed between spheres and rods at any time point (Figure S7, Supporting Information). We hypothesize that a similar percentage of particle uptake of Poly-SA rods and spheres in human blood could be due to the heterogeneity of Poly-SA particle size and variations in each human donor.

Despite the similar percentage of human neutrophils internalizing rods and spheres, Poly-SA rods still showed selectivity for neutrophils. We repeated our particle uptake assay with THP-1 monocytes and found a 77% decrease in phagocytosis of Poly-SA rods over spherical particles, similar to the trend observed with mouse monocytes (Figure S8, Supporting Information).

2.2. Rod-Shaped Poly-SA Particles and Spheres of Equal Volume Modulate Neutrophil Accumulation in the Alveolar Space of Mice with LPS-Induced Lung Injury

Previous studies have demonstrated that spherical carriers phagocytosed by circulating neutrophils interfere with the cells' ability to interact with the inflamed endothelium, consequently reducing neutrophil transmigration.[2,18,19,21] Given neutrophils' preferential and greater uptake of elongated carriers over spherical ones, we hypothesized that using rod-shaped particles could enhance this blockage of neutrophil trafficking to sites of inflammation. To test this hypothesis, we utilized a mouse ALI model to evaluate the impact of Poly-SA elongated particles on neutrophil transmigration during acute inflammation.

BALB/c mice received LPS orotracheally to induce upregulation of leukocyte adhesion molecules on the pulmonary endothelium, which led to neutrophil recruitment to the airspace.[6,35,36] One hour after LPS instillation, we injected mice with ≈20 mg k^{-1} g of 1 μm Poly-SA spheres or rods (4×10^{8} particles per mouse) via tail vein and assessed neutrophil migration to the inflamed lungs 2 h after particle injection. **Figure 2A** shows a schematic for this procedure, where we collected the bronchoalveolar lavage fluid (BALF) and whole blood from mice to determine the number of transmigrated neutrophils into the airspace and circulating neutrophils in the blood.

To assess neutrophil transmigration, we evaluated the total leukocyte count in the BALF, the percentage of neutrophils in the BALF, and the total BALF transmigrated neutrophils (Figure 2B–D). Mice receiving only LPS demonstrated a significant increase in BALF infiltrates compared to healthy controls, indicative of lung inflammation. However, we observed that the intravenous injection of both 1 μm Poly-SA rods and spheres significantly reduced the total leukocyte count in the BALF. Poly-SA rod-treated mice exhibited a 42% decrease in total leukocyte count in the BALF relative to mice receiving only LPS. In contrast, mice treated with Poly-SA spheres showed a 22% reduction of BALF leukocytes (Figure 2B).

The reduction of leukocytes in the BALF of particle-treated mice directly correlated with decreased BALF composition and neutrophil count (Figure 2C,D). BALB/c mice receiving 1 μm Poly-SA rods exhibited a significant reduction in the count of transmigrated neutrophils, with a 59% decrease compared to LPS-only mice and corresponding to 50% of the collected BALF cells. Mice treated with 1 μm Poly-SA spheres also significantly reduced the accumulation of transmigrated neutrophils in ALI

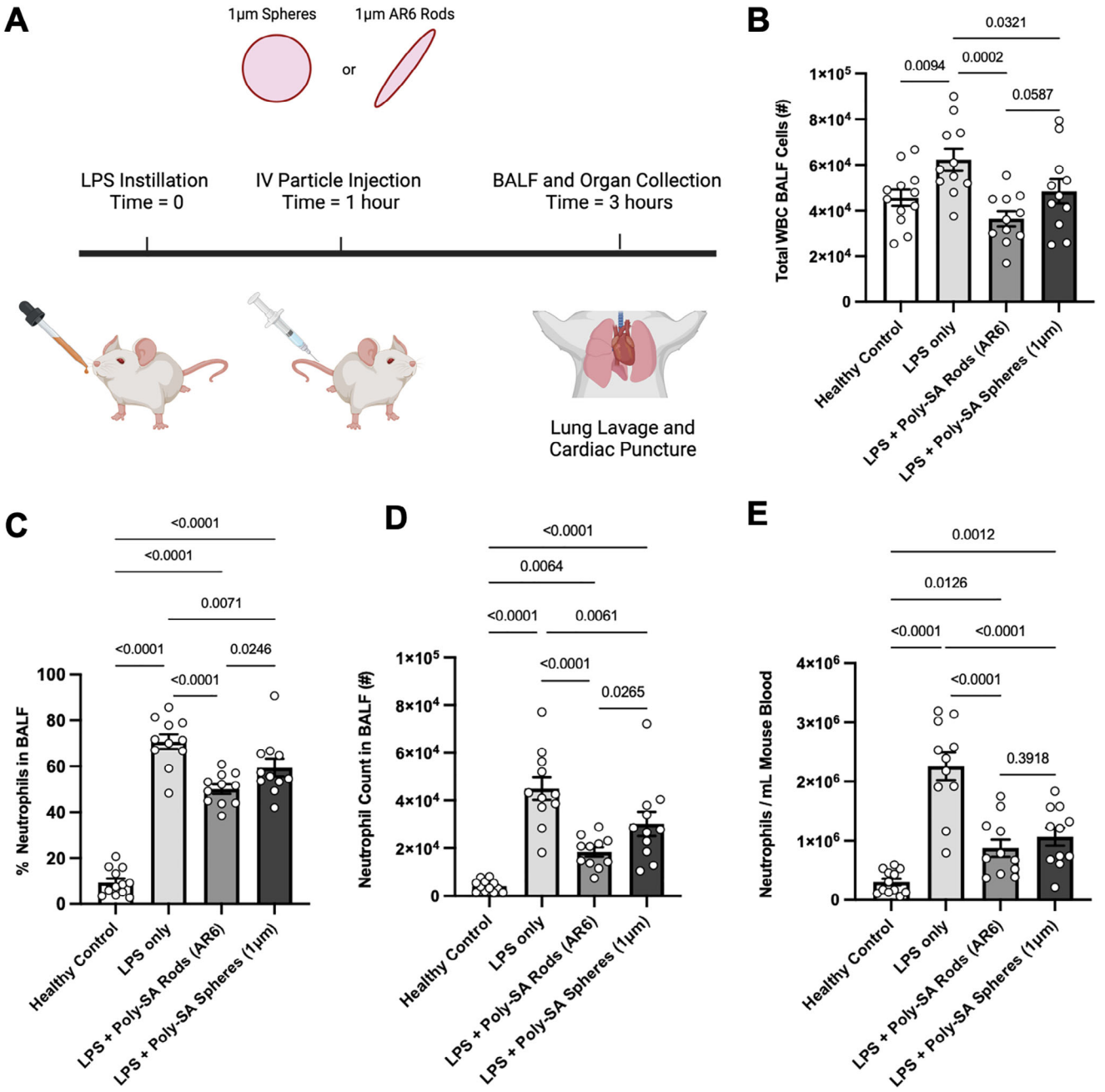

Figure 2. Characterization of neutrophil accumulation in BALF after Poly-SA particle administration in an LPS-induced murine lung injury model. A) Diagram of dosing schedule of LPS instillation and Poly-SA particle intravenous injection on BALB/c mice. B) Average total white blood cell (WBC) count, C) neutrophil population distribution, and D) neutrophil cell count in BALF after particle treatment. E) Neutrophil concentration in mouse blood after LPS instillation and Poly-SA particle administration. Mouse blood was collected via cardiac puncture. The total WBC count and leukocyte cell percentages for mouse blood and BALF were determined using a hemacytometer and flow cytometry, respectively. Statistical analysis was performed with one-way ANOVA with Fisher's LSD test and 95% confidence interval. Circles represent biological replicates obtained from mouse cohorts ($n \geq 11$). Figure 2A was created with BioRender (https://BioRender.com/x54j031).

airspace but to a lesser extent, with a 33% decrease from the LPS-only group and comprising 59% of the BALF cells. Thus, 1 µm Poly-SA rods prevented neutrophil accumulation in the alveolar space more effectively than spheres, representing a 48% difference in average neutrophil count between both groups (Figure 2D). The results suggest that Poly-SA rods might outperform spheres due to rods' enhanced and selective particle phagocytosis.

Next, we sought to evaluate the concentration of neutrophils in blood because previous work shows that circulating leukocyte count can vary after particle treatment due to blood leukocytes parting from injury sites.[18,23,24] As depicted in Figure 2E, local

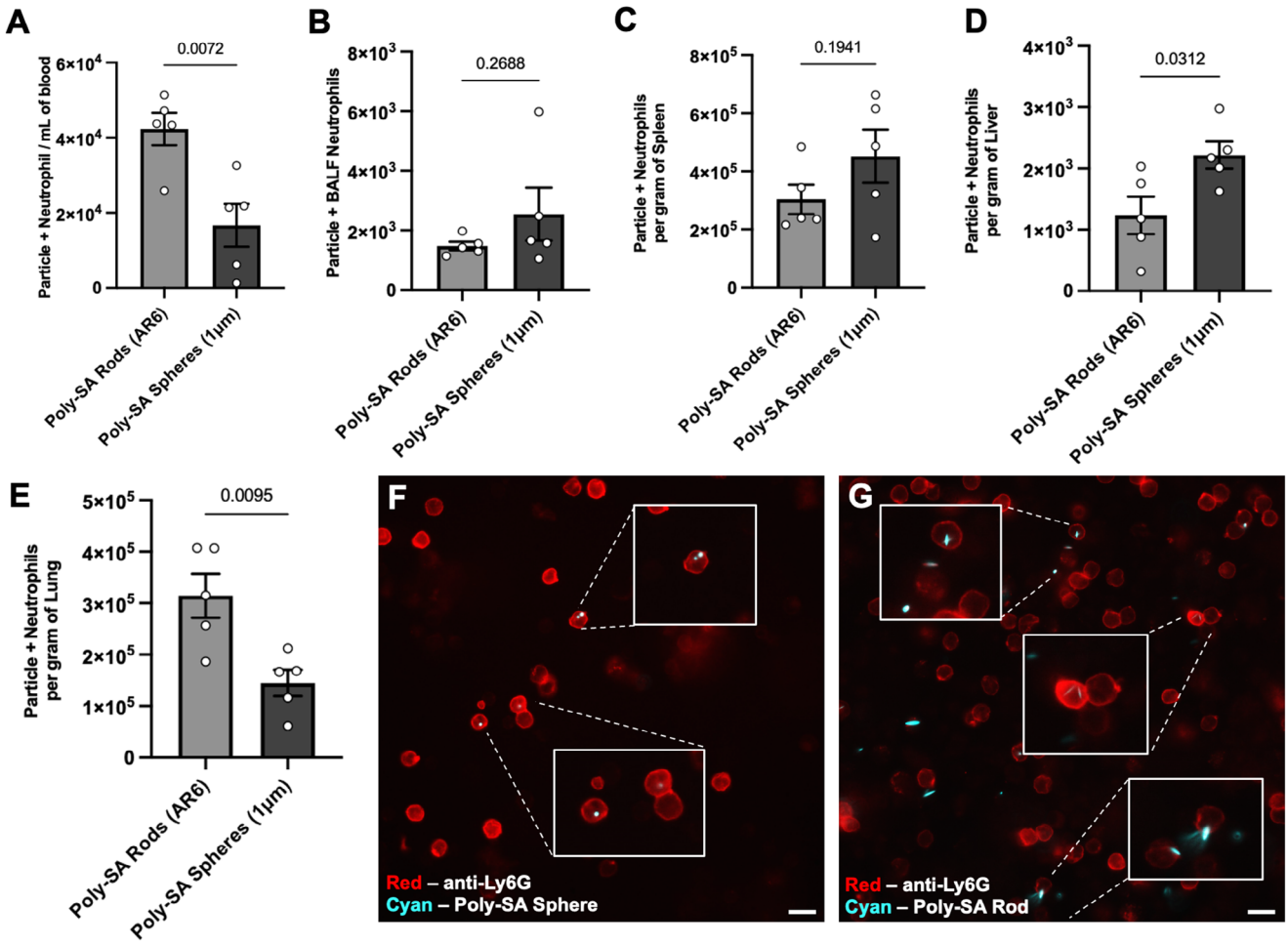

Figure 3. Neutrophil-particle accumulation in blood, BALF, spleen, liver, and lung in an LPS-induced murine lung injury model. Mouse neutrophil population of $CD45^+CD11b^+Ly6G^+$ that is associated with Poly-SA rods or spheres in ALI A) blood, B) BALF, C) spleen, D) liver, and E) lung. Fluorescent images of mouse neutrophils recovered from the lung tissue of mice treated with F) Poly-SA spheres and G) Poly-SA rods. Images represent data from panel (E). Mouse neutrophils are shown in red, and Poly-SA spheres and rods are shown in cyan. We noticed an increased number of neutrophils associated with Poly-SA rods compared to spheres of equal volume in the lung tissue, as seen in the close-up panels. The scale bar for (F,G) is 20 μm. Statistical analysis was done for panels A to E with an unpaired Student's *t*-test. Circles represent biological replicates obtained from mouse organs ($n = 5$).

LPS instillation in the lungs significantly increased circulating neutrophils in the blood of LPS-only mice compared to healthy controls. Treating LPS-injured mice with Poly-SA particles decreased the count of circulating neutrophils by 61% for Poly-SA rods and 53% for Poly-SA spheres compared to the LPS-mice group. We observed no statistical variations in the neutrophil concentration in blood between Poly-SA rod- and sphere-treated mice. This suppression of circulating neutrophils after particle injection is consistent with prior work using polymeric carriers in ALI.[18]

2.3. Mouse Neutrophils Associated with Rod-Shaped Poly-SA Particles Accumulate in the Lung Tissue of LPS-Challenged Mice

Previous studies have determined that neutrophils phagocytosing spherical carriers can divert such cells from injury sites and accumulate them in organs such as the liver and spleen during inflammation.[18,23,24] However, limited information about the cellular-level biodistribution of non-spherical particles is known. Hence, we investigated how elongated particles affect neutrophil distribution among various organs of our ALI mouse model. BALB/c mice received LPS and were treated with Cy5.5-labeled Poly-SA rods or spheres (1 μm) as previously described above. We evaluated the particle-positive neutrophil distribution 2 h after particle treatment using single-cell suspensions collected from the lungs, liver, spleen, blood, and BALF of ALI mice. We identified particle-positive neutrophils in such organs by the positive signal of Cy5.5.

First, we found that circulating mouse neutrophils associated more with 1 μm Poly-SA rods than with Poly-SA spheres of equal volume in vivo, as indicated by the significantly higher cell count (**Figure** 3A) and percentage of blood neutrophils (Figure S9A, Supporting Information) associated with rods relative to spheres. The in vivo results complement the ex vivo outcome shown in Figure 1B. Indeed, the fold increase in neutrophil phagocytosis of

elongated particles compared to spheres was greater in vivo than in ex vivo. Poly-SA rods (1 μm) showed a threefold increase in the percentage of particle-positive neutrophils over 1 μm spheres in vivo (Figure S9A, Supporting Information) compared to the 1.3-fold increase for ex vivo assays (Figure 1B).

Interestingly, we found that particle-positive neutrophils can transmigrate from the blood to the airspace in LPS-challenged mice, indicated by the positive particle signal in the neutrophil BALF population. As shown in Figure 3B, ≈2500 BALF neutrophils were sphere-positive, and ≈1500 were rod-positive. These numbers correspond to ≈15% of BALF neutrophils from Poly-SA sphere-treated mice being particle-positive, while ≈8% of the BALF neutrophils recovered from rod-treated mice were particle-positive (Figure S9B, Supporting Information). The particle-positive neutrophil count and the percentage of particle-positive cells between rods and sphere groups in the BALF were not statistically significant.

Further, we evaluated the distribution of particle-positive neutrophils in the spleen, liver, and lung. As shown in Figure 3C, ALI mice injected with Poly-SA spheres had ≈450 000 particle-positive neutrophils per gram of spleen. Meanwhile, mice treated with Poly-SA rods had ≈300 000 particle-positive neutrophils per gram of organ. These raw counts of particle-positive neutrophils were not significant and represent ≈30% of the total neutrophils recovered from ALI mice spleen particles for both the rods and spheres treatments (Figure S9C, Supporting Information). The total neutrophil counts recovered from all organs and used to compute percent particle positive values are listed in Figure S10 (Supporting Information).

Contrary to the spleen data, we found a significant increase in sphere-positive neutrophils accumulating in the liver compared to rod-positive cells. Specifically, we recovered ≈2200 particle-positive neutrophils per gram of liver of ALI mice treated with Poly-SA spheres compared to ≈1200 particle-positive cells per gram of liver for Poly-SA rod-treated mice (Figure 3D). We confirmed this result using immunofluorescence histological sections of liver samples from Poly-SA-treated mice, where we observed more co-localization of $Ly6G^+$ neutrophils (yellow) and Cy5.5-Poly-SA particles (red) in mice treated with 1 μm spheres compared to rods (Figure S11, Supporting Information). These findings are consistent with prior work demonstrating that neutrophils associated with spherical polymeric particles are found in the liver during LPS-induced lung inflammation.[18,19] These raw counts of particle-positive, though significant, translated to ≈25% of the total neutrophils recovered from the liver tissue associated with Poly-SA rods or spheres (Figure S9D, Supporting Information).

Unlike the liver, we found more total and particle-positive neutrophils accumulating in the lung tissue of mice treated with Poly-SA rods (Figure 3E). Notably, ALI mice treated with Poly-SA rods had a significantly higher number (≈310 000) of particle-positive neutrophils per gram of lung tissue compared to mice treated with Poly-SA spheres (≈140 000), representing 54% more particle-positive neutrophil accumulation in the lung tissue of rod-treated mice compared to sphere-treated ones. We confirmed these findings using fluorescence microscopy images of the neutrophils recovered from the lung tissue (Figure 3F,G) and by examining immunofluorescence images of whole lung sections. The tissue sections revealed a greater accumulation of rod-positive neutrophils in the lung tissue, as indicated by the increased co-localization of $Ly6G^+$ neutrophils (yellow) and Cy5.5-Poly-SA particles (red) in mice treated with Poly-SA rods compared to those treated with spheres (Figure S12, Supporting Information). Approximately 18% of neutrophils recovered from the lung tissue were associated with Poly-SA rods or spheres (Figure S9E, Supporting Information). However, we found a significant increase in the total neutrophil count per mass of lung tissue of ALI mice injected with Poly-SA rods compared to those with spheres (Figure S10C, Supporting Information).

Due to the results obtained from the particle-positive neutrophil tissue distribution, we wondered if the higher neutrophil count associated with Poly-SA rods in the lung tissue was due to rods accumulating in the lungs. As presented in Figure S13 (Supporting Information), our particle biodistribution results indicated that both elongated and spherical Poly-SA particles predominantly localized in the liver and spleen as soon as 30 min after particle injection, similar to prior work using polymeric microparticles.[18,19,22,37,38] Additionally, only ≈10% of the particle fluorescence recovered 2 h after particle injection comes from the lung tissue for both Poly-SA rod- and sphere-treated mice.

While treating LPS-challenged mice with Poly-SA rods resulted in a decrease in neutrophil infiltration into the airspace (Figure 2D), we wondered if the accumulation of rod-positive neutrophils in the lung tissue was potentially due to elevated pro-inflammatory signals from the alveolar space. However, our results showed that Poly-SA-rod mice had minimal differences in cytokine signal in the BALF compared to sphere-treated and LPS-only mice (except for IL-6) (Figure S14, Supporting Information).

In summary, we observed that neutrophils that phagocytosed rod-shaped Poly-SA particles in an LPS-induced lung inflammation model tend to remain in the lung tissue rather than divert to the liver and spleen like their spherical counterparts. Nonetheless, the accumulation of rod-positive neutrophils in the lung tissue did not cause greater neutrophil infiltration to the alveolar space (Figures 2D, and 3E).

2.4. Neutrophils that Phagocytose Rod-Shaped Poly-SA Particles are Less Likely to Transmigrate Across an Endothelial Monolayer

Given the retention of rod-positive neutrophils in the lung tissue and the lower fraction of rod-positive neutrophils found in the BALF of our lung inflammation model (Figure 3; Figure S9, Supporting Information), we questioned if the neutrophil motility from blood to the airspace was potentially hindered after phagocytosis of elongated particles. To answer this question, we utilized an in vitro model of neutrophil transmigration. We assessed the migration ability of particle-loaded neutrophils across a confluent layer of endothelial cells in vitro using a human umbilical vein endothelial cell (HUVEC) monolayer cultured on permeable inserts. After the HUVEC monolayer was fully confluent, we isolated human neutrophils from whole blood and incubated them with rhodamine B-labeled Poly-SA spheres of varying diameters (500 nm, 1 μm, and 2 μm) or their corresponding AR 6 Poly-SA rods for 1 h to allow for phagocytosis. Human neutrophils were used to match the use of human endothelial cells, which are more readily available than mouse cells.

Neutrophils were incubated with Poly-SA particles at particle-to-neutrophil ratios of 16:1 for 2 and 1 μm particles, and 80:1 for 500 nm particles. These ratios were empirically determined and quantified using flow cytometry to maximize the percentage of particle-positive neutrophils. With these particle-to-cell ratios, we target at least 80% of the neutrophil population with either spheres or rods for each particle type (Figure S15A, Supporting Information). Confocal microscopy images (**Figure** 4A,B; Figure S15B, Supporting Information) show that isolated human neutrophils readily internalize the Poly-SA rods and spheres. Moreover, we observed phagocytosis of ≈10 particles per cell for 500 nm rods and spheres, ≈6 particles per cell for 1 μm rods and spheres, ≈4 particles per cell for 2 μm rods, and ≈7 particles per cell for 2 μm spheres (Figure 4C).

Neutrophils pre-treated with Poly-SA particles were added to the upper chamber of the permeable insert, and IL-8, acting as an inflammatory agent, was added to the lower chamber to recruit neutrophils for 1.5 h. As expected, untreated neutrophils migrated across a confluent HUVEC monolayer during an IL-8 gradient (Figure 4D). Conversely, we observed that neutrophils pre-treated with Poly-SA particles of all sizes and shapes showed reduced transmigration. Specifically, neutrophils incubated with Poly-SA spheres exhibited a significant decrease in transmigration compared to untreated cells, corresponding to a 49%, 56%, and 91% reduction for 500 nm, 1 μm, and 2 μm Poly-SA spheres, respectively. Similarly, neutrophils pre-incubated with Poly-SA rods exhibited a 68%, 72%, and 98% reduction in migration over untreated neutrophils for 500 nm, 1 μm, and 2 μm AR 6 Poly-SA rods, respectively. We considered that the reduced neutrophil migration after particle internalization may be due to particle toxicity. Thus, we analyzed the viability of isolated neutrophils after particle uptake for each particle group. Consistent with our prior work,[22,32] we observed minimal cell toxicity after Poly-SA particle treatment, with over 88% neutrophil viability after our particle dosing (Figure S16, Supporting Information).

When considering the percentage of particle-positive cells among the transmigrated neutrophil pool, we found that neutrophils carrying Poly-SA rods of all sizes are less likely to transmigrate than neutrophils loaded with spheres (Figure 4E,F). For neutrophils pre-treated with 500 nm, 1 μm, and 2 μm Poly-SA rods, we found that ≈75%, ≈67%, and ≈40% of the transmigrated cells were rod-positive, respectively. However, ≈98%, ≈93%, and ≈91% of the transmigrated neutrophils from the sphere-treated groups were correspondingly associated with 500 nm, 1 μm, and 2 μm Poly-SA spheres. This indicates that the transmigration of rod-loaded neutrophils across an endothelial layer decreased by 23% (500 nm), 28% (1 μm), and 56% (2 μm) compared to neutrophils carrying spheres of equal volume. These results are notable because the percentage of particle-positive cells and the number of particles internalized by neutrophils were similar for rods and spheres between each tested size (except for 2 μm particles). Therefore, the observed differences in transmigration might be due to the shape of the particle rather than variations in particle-mediated targeting.

Thus far, we have used only the Poly-SA polymer in our in vivo lung injury and in vitro transmigration model. In both instances, we observed that elongated Poly-SA particles alter neutrophil transmigration at the site of inflammation relative to spheres of equal volume, likely due to particle shape effects. To ensure our findings are consistent despite the particle material, we fabricated 2 μm biodegradable poly(lactic-*co*-glycolic acid) (PLGA) spheres and stretched them into 2 μm rods. We selected PLGA because it is a well-studied polymer and a gold-standard material used in medical technologies approved by the United States Federal Drug Administration.[2,39] Table S2 (Supporting Information) shows the characterization of PLGA spheres and rods.

Similar to Poly-SA particles, the internalization of 2 μm PLGA spheres and rods significantly reduced the number of transmigrated neutrophils in our in vitro transmigration model. We observed that for neutrophils pre-treated with PLGA rods, only ≈20% of the transmigrated neutrophil pool was particle-positive, whereas ≈71% of the transmigrated neutrophils in the sphere-treated group were associated with PLGA spheres (Figure S17, Supporting Information). In this case, the transmigration of PLGA rod-loaded neutrophils declined by 73% compared to neutrophils carrying 2 μm PLGA spheres. These results suggest that the observed reduced neutrophil migration might be dominated by the particle shape and not based on the polymer material itself.

Our in vitro transmigration model supports previous findings, demonstrating that phagocytosis of polymeric particles impairs neutrophils' ability to transmigrate during inflammation. Furthermore, it highlights that the shape of the particles, whether spherical or elongated, affects neutrophils' transmigration propensity differently.

2.5. Rod-Loaded Neutrophils Show Decreased Actin Polymerization Following IL-8 Stimulation

We questioned if the reduced motility of rod-loaded neutrophils across an endothelial layer was potentially due to changes in cell deformation, an essential requirement for cell spreading and migration in response to chemotactic gradients.[40,41] Since actin polymerization is required for these morphological changes,[42,43] we evaluated actin distribution and polymerization on particle-loaded neutrophils after exposure to chemoattractant stimulation. Similar to our in vitro transmigration model, we isolated human neutrophils from whole blood and incubated them with Rhodamine B-labeled Poly-SA rods AR 6 (500 nm, 1 μm, and 2 μm) and spheres of equal volume for 1 h to facilitate particle uptake. Neutrophils pre-treated with Poly-SA particles were then stimulated in suspension with IL-8, and we stained and measured F-actin content (**Figure** 5A).

Neutrophils exposed to IL-8 stimuli exhibited rapid actin polymerization, evidenced by forming an actin ring network in contrast to unstimulated neutrophils, as observed in confocal microscopy images. Additionally, flow cytometry analysis highlighted an increase in overall F-actin content in IL-8-activated neutrophils relative to unstimulated cells (Figure 5B). Interestingly, we observed that neutrophils pre-treated with Poly-SA spheres of all sizes showed reduced F-actin content after IL-8 exposure. Activated sphere-loaded neutrophils showed a significant reduction in total F-actin content relative to IL-8-stimulated no-particle control, corresponding to a 24%, 18%, and 31% decrease for 500 nm, 1 μm, and 2 μm Poly-SA spheres, respectively. Likewise, activated rod-loaded neutrophils exhib-

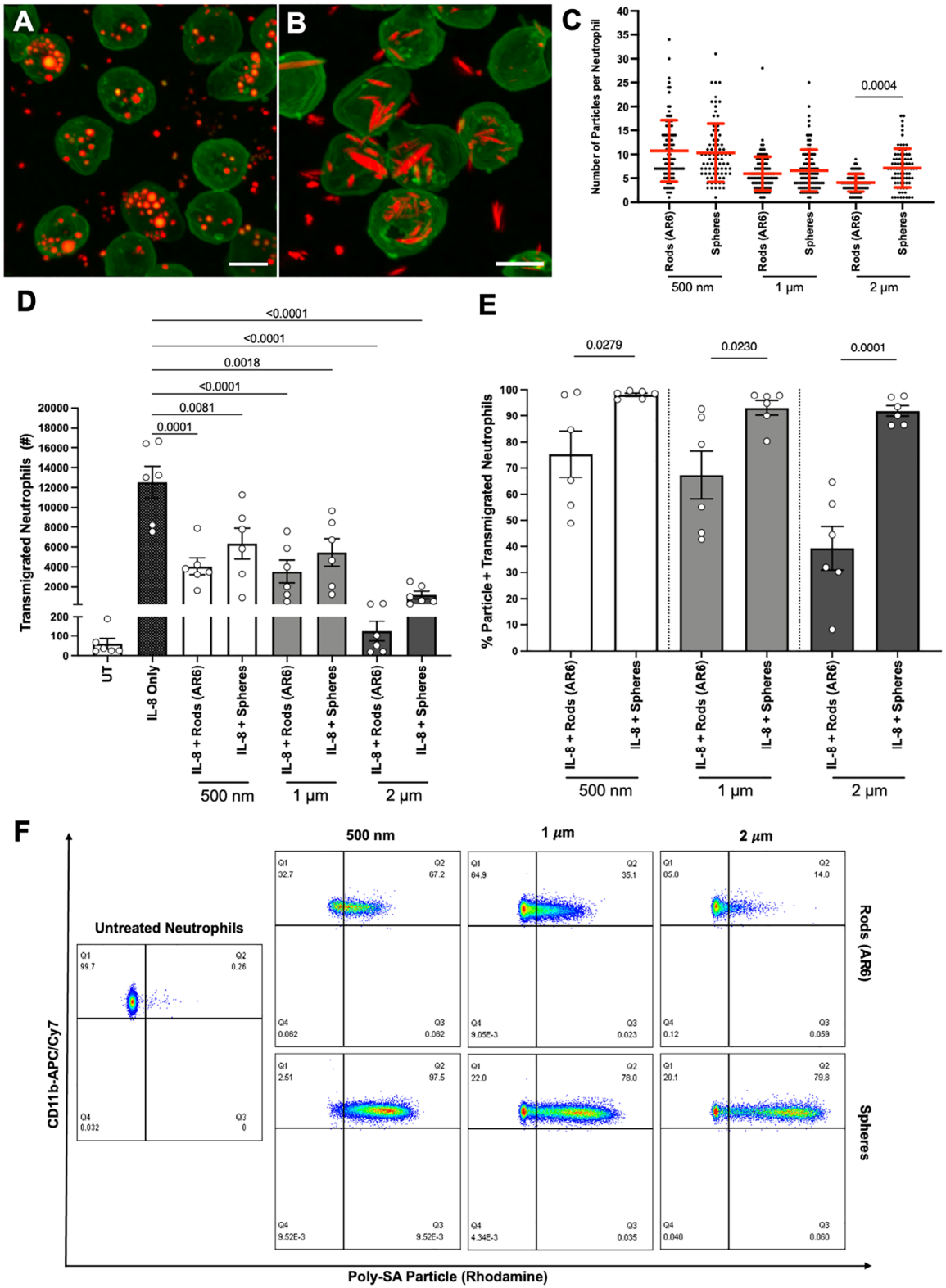

Figure 4. Human Neutrophil Transmigration across a HUVEC Monolayer after Poly-SA Particle Uptake. Isolated human neutrophils were incubated with rhodamine-labeled Poly-SA particles for 1 h at 37 °C and 5% CO_2 before placement on a HUVEC monolayer. Confocal microscopy images of isolated human neutrophils incubated with rhodamine-labeled A) Poly-SA 1 µm spheres and B) Poly-SA 1 µm AR 6 rods. Particles are labeled red (Rhodamine B), and neutrophils are labeled green (Alexa Fluor 488 – Wheat Germ Agglutinin). Scale bars are 10 µm. Images showcase the maximum intensity projection. C) Distribution of Poly-SA particle uptake per isolated human neutrophils. Confocal microscopy images of at least 80 neutrophils per particle group were

used to determine the particle per cell count. Particle-treated neutrophils were allowed to transmigrate across a HUVEC monolayer and an IL-8 gradient for 1.5 h at 37 °C and 5% CO_2 before cell collection in the lower compartment. Collected neutrophils were stained with anti-human CD11b to determine D) the total number of transmigrated neutrophils and E) the percentage of particle-positive transmigrated neutrophils using flow cytometry. F) Representative flow cytometry plots showing the percentage of neutrophils associated with either Poly-SA spheres or Poly-SA rods (AR6) after transmigration. Statistical significance between groups was determined with (C,D) One-way ANOVA with Tukey's post-test and E) unpaired Student's *t*-test. Circles represent data collected from healthy blood donors ($n = 6$).

ited a 43%, 22%, and 42% reduction in F-actin content compared to stimulated no-particle neutrophils for 500 nm, 1 µm, and 2 µm AR 6 Poly-SA rods, respectively (Figure 5C). Notably, the rod-loaded neutrophils consistently had significantly less F-actin content than neutrophils carrying the equivalent-sized spheres (Figure 5C,D). F-actin in neutrophils pre-treated with 500 nm, 1 µm, and 2 µm Poly-SA rods after stimulation with IL-8 significantly decreased by 24%, 5%, and 16% compared to activated neutrophils carrying spheres of equal volume, respectively.

Figure 5D and Figure S18 (Supporting Information) noted differences in the F-actin distribution and signal intensity between IL-8-activated neutrophils pre-treated with Poly-SA spheres versus rods. Stimulated sphere-loaded neutrophils typically exhibit uniform and bright F-actin ring structures. In contrast, rod-loaded neutrophils show dispersed and dim F-actin, particularly in cells treated with 500 nm and 2 µm.

Finally, we found no statistical differences in F-actin content among unstimulated neutrophils treated with rods, spheres, or no particles across all examined carrier sizes (Figure S19, Supporting Information). We also assessed the F-actin levels in IL-8-stimulated neutrophils loaded with PLGA particles. Our findings revealed that neutrophils containing 2 µm PLGA rods exhibited a 30% reduction in F-actin content compared to the stimulated neutrophils with 2 µm PLGA spheres (Figure S20, Supporting Information). Our findings suggest that the observed difference in actin polymerization between rod- and sphere-loaded neutrophils after IL-8 exposure is primarily influenced by particle shape rather than baseline actin measurements or polymeric material.

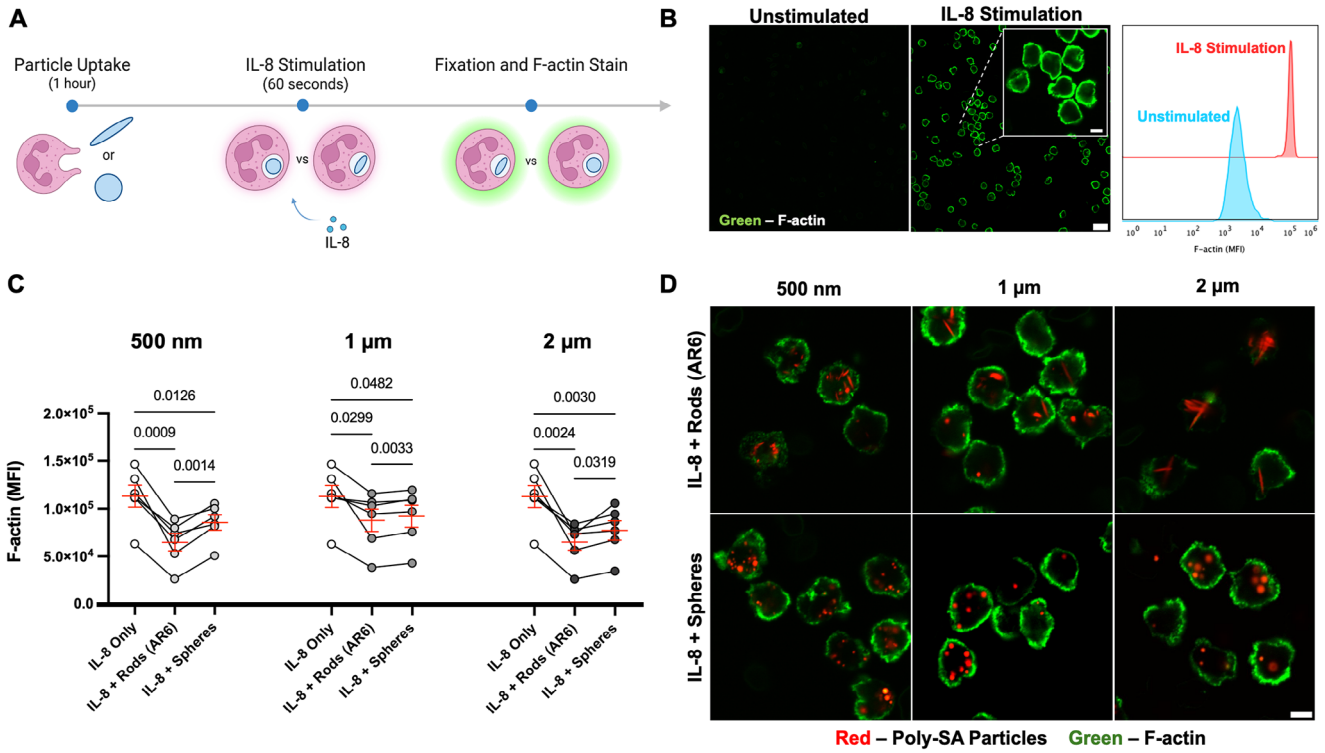

Figure 5. Characterization of F-actin in Particle-loaded Human Neutrophils After IL-8 Stimulation. A) Illustration showing the workflow for assessing F-actin in Poly-SA-treated human neutrophils following IL-8 stimulation. B) Confocal microscopy images of isolated human neutrophils stimulated with or without IL-8 for 60 s in suspension. Neutrophils are fixed, permeabilized, and stained for F-actin (ActinGreen 488 ReadyProbes). IL-8 stimulation induced rapid actin polymerization, as evidenced by the formation of cortical actin (green) and an overall increase in F-actin signal as measured by flow cytometry. Scale bars indicate 5 µm (for the close-up image) and 20 µm. C) The F-actin content of neutrophils pre-treated with Poly-SA rods (AR6) and spheres, followed by IL-8 stimulation, is represented as the mean fluorescence intensity (MFI). D) Confocal microscopy images showing the distribution of F-actin in neutrophils treated with Poly-SA rods and spheres, followed by IL-8 stimuli. Poly-SA particles are shown in red (Rhodamine B), and F-actin in green. The scale bar is 5 µm. Statistical significance between groups was assessed using a One-way Repeated Measures ANOVA followed by Fisher's LSD post-test for (C). Circles represent individual healthy blood donors ($n = 6$), and a horizontal red line indicates the average data and standard error of the mean (SEM) in (C). White circles indicate the same IL-8-only donor control across all particle sizes. Figure 5A was created with BioRender (https://BioRender.com/c28z131).

3. Discussion

Particulate drug carriers delivered intravenously typically undergo rapid clearance from the bloodstream and accumulate in the reticuloendothelial system (RES) organs such as the liver and the spleen, where phagocytic resident macrophages are highly efficient at clearing carriers from the body.[2] The short circulation time and rapid phagocytic clearance of particulate carriers often limit the efficacy of particle-based therapies intending to reach tissues and cell types other than those from the RES.[2,44] Hence, researchers have carefully considered particle design to improve the targeting of desired tissue and cells. Particle geometry has become an essential parameter in particulate carrier design because it influences various biological interactions, including particle phagocytosis,[27,45] particle margination,[33,38,46] and circulation time.[47,48] Particle geometry can also be utilized to influence the mechanotransduction pathways and behavior of cells for tissue engineering and regenerative medicine applications. Adding microstructures, such as micro-rods, to scaffolds or infarct tissues influences fibroblast proliferation and phenotype, thereby modulating fibrotic responses.[49,50] Moreover, the dimensions of these microstructures also influence fibroblast differentiation, with microfibers with a high aspect ratio reducing myofibroblast proliferation and, hence, fibrotic encapsulation surrounding the microstructure.[51]

Recent literature reveals that modifying the particle geometry – from spherical to elongated – could improve neutrophil targeting via phagocytosis and offer promising results for treating neutrophilic inflammation.[27] To our knowledge, this work uniquely investigates the impact of cargo-free, anti-inflammatory Poly-SA rod-shaped particles on neutrophil transmigration to areas of inflammation relative to their spherical counterparts in vivo and in vitro.

Interestingly, our data reveal differences between human and mouse neutrophil uptake of Poly-SA rods and spheres. Our work indicates that mouse neutrophils significantly phagocytosed more Poly-SA rods of all sizes than their corresponding spherical carriers. In contrast, primary human neutrophils phagocytose Poly-SA rods and spheres to the same extent. Despite the similar targeting ability of both particle types, we demonstrated that targeting human neutrophils with elongated Poly-SA particles still offers an advantage over spheres because of other phagocytes' reduced interaction with elongated carriers, as observed with human model monocytes, THP-1 cells. Similarly, our work suggests that neutrophil uptake of elongated particles might be enhanced in inflow conditions. Given the improved vascular wall targeting of non-spherical particles compared to spherical ones,[46,52] we hypothesize that enhanced targeting of neutrophils in vivo is because elongated carriers might interact more with marginated neutrophils inflow since they are localizing in the same space, leading to particle phagocytosis. Likewise, our results align with prior work that demonstrated the uptake of 500 nm polystyrene rods over 500 nm spheres was greater in vivo than in ex vivo.[27]

Intravenous delivery of Poly-SA spheres and rods resulted in a considerable reduction of neutrophil trafficking to the airspace of mice lungs; however, 1 μm Poly-SA rods outperformed Poly-SA spheres of equal volume. We speculate that the observed differences in blocking neutrophil trafficking in vivo between Poly-SA rods and spheres are mainly driven by particle geometry, enhancing neutrophil phagocytosis of rods rather than differences in therapeutic performance. The added anti-inflammatory benefit of Poly-SA spheres has been attributed to the particles' ability to change neutrophils' surface expression of inflammatory molecules, for example, CD62-L, after particle phagocytosis.[19] Since 1 μm Poly-SA rods are derived from 1 μm Poly-SA spheres and hold the same salicylic acid content, we expected that elongated and spherical Poly-SA particles would perform similarly at preventing neutrophil activation. Additionally, our earlier studies indicate that free aspirin does not halt neutrophil migration to the airspaces of lungs infected by endotoxins or bacteria, nor does it change the adhesion of neutrophil-platelet aggregates to inflamed endothelium during thromboinflammation.[19,22] This highlights the importance of particle phagocytosis by activated neutrophils in efficiently altering cell behavior from the "inside out."

The literature suggests that particle geometry influences carriers' biodistribution. Non-spherical particles such as filomicelles, silica, or gold nanoparticles generally exhibit reduced liver accumulation and collect in other organs, such as the lungs and spleen.[48,53–55] However, limited studies have assessed the cellular-level biodistribution of non-spherical particles.[27,56] Prior work has demonstrated that particle-positive neutrophils are found in the liver of ALI mice when treated with 500 nm and 2 μm polymeric spheres.[18] However, our results revealed that neutrophils that phagocytosed 1 μm Poly-SA rods were localized in the lung tissue of ALI mice. In contrast, neutrophils that internalized 1 μm Poly-SA spheres were found in the liver. Potentially, neutrophils could phagocytose particles already captured in organs collected in this study. However, if phagocytosis were to happen due to particle accumulation, we would expect an increase in rod-positive neutrophils in all organs recovered, especially in the liver and spleen, because of neutrophils' enhanced uptake of elongated particles. We speculate that the accumulation of rod-positive neutrophils in the lung tissue is most likely not due to particle phagocytosis at the site (lungs) but neutrophils internalizing elongated particles in circulation to be retained later in the lung tissue. Thus, our data suggest particle geometry might affect the biodistribution of particle-positive neutrophils in ALI mice.

We investigated whether neutrophil phagocytosis of non-spherical particles affects cell motility at the inflammation site, hoping to explain the accumulation of rod-positive neutrophils in the inflamed lungs. Prior work by Habibi et al. elucidated that particle properties can impact the transmigration ability of nanoparticle-loaded THP-1 monocytes across a blood–brain barrier model. The study alluded to the total mass of particles taken by the cells and the mechanical properties of such particles affecting cell movement and their migration behavior across a barrier.[57] Our in vitro results reveal that rod-loaded neutrophils were less likely to transmigrate through an endothelial monolayer than neutrophils treated with spheres of equal volume. Our results imply that particle geometry is the driving factor for the reduced transmigration ability of rod-loaded over sphere-loaded neutrophils because the percentage of particle-positive cells and the extent of phagocytosis (e.g., particle number inside the cell) were the same between rod- and sphere-treated cells. Likewise, we found that the reduced transmigration ability of rod-loaded neutrophils was independent of the particle material.

In our in vitro work, we demonstrate that rod-loaded neutrophils have reduced F-actin content compared to sphere-loaded or no-particle-treated neutrophils after stimulation with IL-8. This greater reduction in actin levels in rod-loaded neutrophils after stimulation than in sphere-loaded cells may account for their low motility at inflammation sites, as these cells likely have decreased polarity and formation of protrusions needed to initiate the migration process.[42,43] For example, megakaryoblastic leukemia 1 (MKL1)-deficient primary human neutrophils demonstrate a distinct impairment in actin polymerization, resulting in a lack of neutrophil spreading and transendothelial migration.[58] Moreover, the shape of the cells and the distribution of F-actin influence neutrophil locomotion during chemotaxis, with neutrophil polarization being essential for cell migration.[59,60]

We also find neutrophils containing Poly-SA spheres have reduced F-actin levels compared to untreated cells after IL-8 activation. Since proper rearrangement of the actin cytoskeleton is crucial for many neutrophil functions, including NET formation,[61] these findings build on our earlier research showing that neutrophils treated with Poly-SA spheres exhibit decreased NET formation upon stimulation with LPS or PMA.[32] The decreased neutrophil NET formation was linked to their uptake of the Poly-SA spheres and the resulting intracellular released salicylic acid inhibiting c-Jun N-terminal Kinase phosphorylation (p-JNK). This impact of Poly-SA spheres on NETs was further confirmed in vivo, where mice treated with Poly-SA had a marked reduction in plasma CitH3, a well-known component of NETs, versus no treatment in a mouse model of DVT.

Other mechanisms could also contribute to the retention and reduced motility of rod-loaded neutrophils across an endothelial layer. One mechanism relates to cell stiffness; phagocytosis of high AR particles might increase the cell stiffness compared to spherical particles of the same volume, decreasing the cell deformability, an important requirement for neutrophil migration.[62] Zak et al. demonstrated that neutrophils become stiffer after phagocytosis of spherical particles,[63] but no direct comparison has been made with non-spherical particles. Likewise, prior work has reported that leukocyte sequestration is partly caused by the increased neutrophil stiffness triggered by inflammatory mediators, transiently reducing cell deformability and, thus, increasing neutrophil retention at sites of injury.[64] Consequently, we would expect to observe a high count of rod-positive neutrophils at the migration sites, as seen in the lung tissue of our LPS-challenged mice. Although neutrophil rigidity is commonly linked to F-actin assembly,[65–67] our findings revealed impaired actin polymerization in rod-loaded cells upon stimulus exposure. Effective cell migration, however, relies in part on actin dynamics, which involve both actin polymerization and depolymerization. Thus, it is important to note that our experiments did not account for actin kinetics in physiological conditions, such as cell spreading and deformation through narrow capillaries or endothelial gaps. Furthermore, we did not consider the synchronized effects of exposure to a chemoattractant and particle uptake on actin kinetics.

A second mechanism relates to blocking access across the endothelial layer; rod-loaded neutrophils cannot physically pass through the endothelial barrier because particles are solid obstacles, causing retention of rod-positive neutrophils at the injury site. It has been reported that the endothelial gap diameters range from 0.2 to 1.4 µm in the venules after exposure to inflammatory stimuli.[68,69] However, the rod-shaped particles have major axes of 6 µm (2 µm rods), 4 µm (1 µm rods), and 2 µm (500 nm rods). Hence, elongated particles might be solid obstacles preventing rod-loaded neutrophils from passing through the endothelial gap. Indeed, our data suggest that the major axes dimensions, and not necessarily the particle volume, modulate the ability of particle-loaded neutrophils to penetrate the endothelial barrier.

Our work demonstrates that elongated polymeric carriers are promising particulate systems for particle-mediated targeting of activated neutrophils. Our results showcase the impact of rod-shaped particles in effectively blocking neutrophil trafficking to inflamed tissue due to the preferential and improved neutrophil uptake of elongated carriers. Furthermore, we showed that particle geometry influences neutrophil function beyond phagocytosis, revealing that neutrophils' internalization of elongated particles might modulate the cell motility across a vascular barrier due to hindered actin polymerization. Understanding mechanism by which shaped particles influence neutrophil motility is imperative for techniques that rely on neutrophil hitchhiking or neutrophil-mediated cargo delivery across vascular barriers, particularly for targeting disease sites and tumor microenvironments.[26,70–72] Indeed, our findings point to more detailed studies of particle-loaded neutrophil migratory ability in more complex structures that incorporate 3D microenvironments and blood flow to more closely resemble vascular regions. Likewise, a library of aspect ratios, particle material, size, and elasticities can be evaluated as unique parameters in particle design that can modulate the migratory ability of neutrophils.

4. Experimental Section

Study Approvals: Human blood was obtained from healthy donors, including 18-30-year-old female and male donors. No sex differences were considered in this study. Informed and written consent was obtained from each donor before the blood draw following protocol #HUM00013973, approved by the University of Michigan Internal Review Board (UM-IRB). All participants were compensated monetarily for each blood donation.

Human umbilical cords were collected from the Mott Children's Hospital, Ann Arbor, under the UM-IRB protocol (# HUM00026898).

Animal studies were conducted according to the National Institute of Health Guidelines for the Care and Use of Laboratory Animals and protocol (#PRO00010572) approved by the Institutional Animal Care and Use Committee of the University of Michigan. BALB/c male mice 7–8 weeks old were purchased from Jackson Laboratories and kept in pathogen-free conditions at the University of Michigan, Ann Arbor.

Fabrication of Poly(Anhydride-Ester) or Salicylic Acid-Based (Poly-SA) Spherical Particles: Poly-SA spherical particles were fabricated using an emulsion solvent evaporation technique. All Poly-SA particles were fabricated with Poly-SA polymer of 8–15 kDa with an adipic acid linker. For 500 nm particles, the oil phase consisted of 10 mg of Poly-SA polymer dissolved in 20 mL of dichloromethane. The oil phase was emulsified into a 75 mL water phase of 2% poly(vinyl alcohol) (PVA, Sigma-Aldrich) at 6000 rpm using an overhead mixer (Caframo). For 1 µm particles, 20 mg of Poly-SA polymer was dissolved in 20 mL of dichloromethane and emulsified into 75 mL of 1% PVA at 4250 rpm. For 2 µm particles, 40 mg of Poly-SA polymer was dissolved in 10 mL of dichloromethane and emulsified in 75 mL of 1% PVA at 4250 rpm. All particle types were stirred for 2 h to allow for solvent evaporation. Poly-SA particles were washed with

deionized water and recovered via centrifugation. Poly-SA spherical particles were lyophilized and stored at −40 °C until further use.

Fluorescently labeled Poly-SA particles were fabricated as stated above, except the oil phase contained either Rhodamine B (≈0.05 mg per mg of Poly-SA polymer, Sigma-Aldrich) or Cy5.5-labeled Poly-SA polymer (≈0.01 mg Cy5.5-labeled polymer per mg of Poly-SA polymer). The Cy5.5-labeled polymer was fabricated as previously described.[19]

Particle morphology and size were determined via scanning electron microscopy (SEM) and ImageJ. The average particle size was determined by measuring the diameter of at least 100 particles. The surface charge of Poly-SA spheres was determined using a Zetasizer (Malvern Zetasizer Nano ZS), and measurements were taken in deionized water.

Fabrication of Poly-SA Rod-Shaped Particles: Poly-SA spherical particles were stretched to rod-shaped particles in one dimension using a heat film-stretching protocol. The particle film was prepared by mixing 3 mg of 500 nm, 1 µm, or 2 µm Poly-SA spheres in 10 mL of 7% PVA. The particle/PVA solution was poured into a single-well plate (Nunc OmniTray) and dried at 60 °C for ≈3 h. The particle film was cut into 1.7 cm × 5 cm sections and stretched at 120 °C using a syringe pump. The AR of the Poly-SA particles was adjusted by modifying the total draw volume of the pump. All Poly-SA spheres were stretched to a fixed AR 6.

The resultant rod-shaped Poly-SA particles were recovered by dissolving the films in deionized water and centrifuged at 4000 rpm for 15 min. Three to four washes with deionized water were performed to remove excess PVA from the particles' surfaces.

The dimensions of rod-shaped particles were determined from SEM images, and the AR was measured using ImageJ. The AR was determined by measuring the length of the major and minor axes of the rods (AR = Major Axis/Minor Axis) of at least 100 representative particles. The surface charge of Poly-SA rods was determined using a Zetasizer.

Fabrication of PLGA Spherical Particles: PLGA spheres (2 µm) were formulated using an emulsion solvent evaporation method. PLGA polymer (acid terminated, lactide: glycolide 50:50, molecular weight 24–38 kDa, Sigma-Aldrich) was dissolved in dichloromethane at a concentration of 2 mg mL^{-1} (oil phase). Twenty milliliters of the oil phase were emulsified in 90 mL of 1% PVA at 2600 rpm for 2 h using an overhead mixer (Caframo). PLGA particles were recovered via centrifugation after repeated washes with deionized water at 4000 rpm for 7 min. PLGA particles were lyophilized and stored at −40 °C until use.

Fluorescently labeled PLGA particles were fabricated as stated above, except the oil phase contained Rhodamine B (≈0.05 mg per mg of PLGA polymer, Sigma-Aldrich). Particle size was determined via SEM and ImageJ. The reported average size was obtained by measuring the diameter of at least 100 particles. The PLGA spheres' surface charge was measured using a Zetasizer.

Fabrication of PLGA Rod-Shaped Particles: PLGA spheres (2 µm) were stretched using a heat film-stretching technique. PLGA spheres (3 mg) were mixed in 10 mL of 7% PVA and poured into a single-well plate. The particle/PVA mix was dried at 60 °C for ≈3 h before stretching. The particle film was cut into 1.7 cm × 5 cm sections and stretched at 120 °C using a syringe pump. All PLGA spheres were stretched to a fixed aspect ratio. The rod-shaped PLGA particles were recovered via centrifugation at 4000 rpm for 15 min.

The dimensions of rod-shaped particles were determined from SEM images and ImageJ. The AR was determined by measuring at least 100 representative particles. The surface charge of PLGA rods was measured using a Zetasizer.

Cumulative Salicylic Acid Release from Poly-SA Spheres and Rods: Non-fluorescent Poly-SA spheres and rods were resuspended in 1× PBS-/- to a final concentration of 10^9 particles mL^{-1}. The particle solutions were rotated for 10 days at 37 °C, and the degradation media were collected at specific intervals. The absorbance measurements were obtained at $\lambda = 295$ nm via UV–vis spectroscopy. The estimation of salicylic acid released from particles was calculated against a 9-point calibration curve of known concentrations of salicylic acid. All standards were also prepared in 1× PBS-/-.

Ex Vivo Uptake of Poly-SA Rods and Spheres by Human Neutrophils: Human whole blood was acquired via venipuncture and immediately anticoagulated with heparin. For Poly-SA rods and spheres uptake Rhodamine B-labeled particles were added to 100 µL of human whole blood to a final concentration of 10^7 particles mL^{-1}. Samples were incubated at 37 °C and 5% CO_2 for 2 h. After 2 h, samples were placed on ice and stained with anti-human CD11b (0.05 µg $sample^{-1}$, Brilliant Violet 421, BioLegend) and anti-human CD62L (0.05 µg $sample^{-1}$, APC/Cy7, BioLegend) for 30 min. Afterward, 2 mL of 1-step Lyse/Fix solution (eBiosciences) was added to each sample for 30 min. The resultant fixed leukocytes were recovered via centrifugation at 500 rcf for 5 min and washed with fluorescence-activated cell sorting (FACS) buffer (1X PBS-/- with 2% heat-inactivated fetal bovine serum (FBS)). The percentage of particle-positive neutrophils was quantified via flow cytometry (Attune CytPix).

To assess CD62L expression on human neutrophils, samples were treated with LPS (0.01 µg $sample^{-1}$, Sigma-Aldrich) for 30 min at 37 °C and 5% CO_2 prior to particle addition. Then, 10^7 particles mL^{-1} of blood were added and incubated for up to 2 h at 37 °C and 5% CO_2. Samples were processed and analyzed as mentioned above.

Ex Vivo Uptake of Poly-SA Rods and Spheres by Mouse Neutrophils and Monocytes: Whole blood from BALB/c male mice (7,8 weeks old) was obtained via cardiac puncture and immediately anticoagulated with heparin. For Poly-SA rods and spheres uptake, Rhodamine B-labeled particles were added to 100 µL of mouse whole blood to a final concentration of 10^7 particles mL^{-1}. Samples were incubated at 37 °C and 5% CO_2 for 2 h. After incubation, samples were placed on ice and stained with anti-mouse CD11b (0.25 µg $sample^{-1}$, FITC, BioLegend), anti-mouse Ly6G (0.1 µg $sample^{-1}$, APC, BioLegend), and anti-mouse Ly6C (0.1 µg $sample^{-1}$, Brilliant Violet 421, BioLegend) for 30 min. Next, 2 mL of 1-step Lyse/Fix solution was added to each sample for 30 min to lyse red blood cells and fix leukocytes. Each sample was washed with FACS buffer at 500 rcf for 5 min. The percentage of particle-positive mouse neutrophils and monocytes was quantified via flow cytometry.

Uptake of Poly-SA Rods and Spheres by THP-1 Monocytes: THP-1 monocytes (ATCC) were grown in RPMI-1640 medium supplemented with 10% FBS at 37 °C and 5% CO_2. Cells were maintained according to the manufacturer's instructions. For Poly-SA rods and spheres uptake, 10^5 THP-1 monocytes were incubated with 10^6 Rhodamine B-labeled particles at 37 °C and 5% CO_2 for 2 h. Next, cells were fixed with 2 mL of 4% paraformaldehyde (Thermo Scientific) for 15 min and washed with FACS buffer at 500 rcf for 5 min. Particle uptake by THP-1 monocytes was determined via flow cytometry.

Acute Lung Injury Model and Poly-SA Particle Treatment: BALB/c male mice were briefly anesthetized using isoflurane to orotracheally deliver LPS to the lungs (50 µL of 0.4 mg mL^{-1}). One hour after instillation, mice were injected via tail vein with 4×10^8 particles per 100 µL PBS-/- (≈20 mg particles kg^{-1} of mice). Mice received either 1 µm Poly-SA spheres or 1 µm Poly-SA AR 6 rods. Two hours after particle injection, mice were euthanized via CO_2 asphyxiation and organs were harvested. Blood was collected from each mouse via cardiac puncture, and lungs were lavaged with ≈1 mL of PBS-/- three times and kept on ice until use. The BALF was centrifuged at 500 rcf for 5 min to collect leukocytes found in the air space, and the supernatant was stored at −80 °C for ELISAs.

Leukocyte count and composition in mouse blood and BALF were determined via hemacytometer (Turk Blood Diluting Fluid) and flow cytometry, respectively. Mouse blood was stained with anti-mouse CD45 (0.1 µg $sample^{-1}$, Brilliant Violet 711, BioLegend), anti-mouse Ly6G (0.1 µg $sample^{-1}$, APC, BioLegend), anti-mouse CD11b (0.1 µg $sample^{-1}$, FITC, BioLegend), and anti-mouse Ly6C (0.1 µg $sample^{-1}$, Brilliant Violet 421, BioLegend). The BALF was stained with anti-mouse CD45 (0.1 µg $sample^{-1}$, Brilliant Violet 711, BioLegend), anti-mouse Ly6G (0.1 µg $sample^{-1}$, APC, BioLegend), anti-mouse CD11b (0.1 µg $sample^{-1}$, FITC, BioLegend), and anti-mouse CD11c (0.1 µg $sample^{-1}$, Brilliant Violet 421, BioLegend). Before flow cytometry, all stained samples were treated with 2 mL of 1-step Lyse/Fix to fix the white blood cells and lyse red blood cells. Each sample was washed with FACS buffer at 500 rcf for 5 min prior to flow cytometry.

Biodistribution of Poly-SA Spheres and Rods in an Acute Lung Injury Model: Male BALB/c mice were challenged with LPS and 10^8 Cy5.5-conjugated 1 µm Poly-SA rods or spheres per 100 µL PBS-/- were administered as dis-

cussed previously. Mice were euthanized at 30 min or 2 h post-particle injection, and organs were harvested to assess the accumulation of particles in vivo. Whole organs (lungs, liver, heart, kidneys, spleen) and blood were collected and scanned using an Odyssey CLx Infrared Imaging System (LI-COR). Samples were scanned using the 700 nm channel with 169 µm resolution to determine the total fluorescence for each organ in the region of interest. Each organ's fluorescence was subtracted from its corresponding untreated or blank organ to account for the organ's autofluorescence. The percentage of fluorescence recovered was determined by calculating the net organ fluorescence divided by the total mean fluorescence of all organs for each mouse.

In Vivo Analysis of Particle-Positive Neutrophil Distribution in an Acute Lung Injury Model after Poly-SA Particle Treatment: As previously described, BALB/c mice were challenged with LPS and 4×10^8 1 µm Cy5.5-conjugated Poly-SA rods or spheres were given intravenously. Mice were euthanized at 2 h post-particle injection and whole organs (lungs, liver, and spleen), blood, and BALF were collected.

Mouse blood and BALF were processed as discussed before. Mouse blood was stained with anti-mouse CD11b (0.1 µg sample^{-1}, FITC, BioLegend), anti-mouse Ly6G (0.1 µg sample^{-1}, Brilliant Violet 605, BioLegend), and anti-mouse Ly6C (0.1 µg sample^{-1}, Brilliant Violet 421, BioLegend). The BALF was stained with anti-mouse CD45 (0.1 µg sample^{-1}, Brilliant Violet 421, BioLegend), anti-mouse Ly6G (0.1 µg sample^{-1}, FITC, BioLegend), and anti-mouse CD11c (0.1 µg sample^{-1}, PE/Cy7, BioLegend).

Whole organs (lungs, liver, and spleen) were kept on cold RPMI-1640 medium until processed. Lungs (right lobe), liver (median lobe), and whole spleen from each mouse were incubated with collagenase (Gibco, Type IV) and DNase (Millipore Sigma) for 30 min, and tissues were processed using a gentleMACS. Samples were strained with a 70 µm mesh and leukocytes were isolated using Lymphoprep (STEMCELL Technologies). The resultant cell suspensions were stained with anti-mouse CD11b (0.1 µg sample^{-1}, FITC, BioLegend), anti-mouse Ly6G (0.1 µg sample^{-1}, Brilliant Violet 605, BioLegend), and anti-mouse CD45 (0.1 µg sample^{-1}, Brilliant Violet 421, BioLegend). Leukocyte count and composition in tissues were determined as $CD45^+CD11b^+Ly6G^+$ using flow cytometry.

In Vitro Neutrophil Transmigration after Particle Uptake: The ability of neutrophil transmigration after phagocytosis of Poly-SA rods or spheres was evaluated using a transwell cell migration assay. Polycarbonate 12-well transwell permeable inserts (3 µm pore size, Corning) were treated with collagen prior to cell seeding. One milliliter of 0.01% v/v calf collagen in 70% ethanol was added to each insert and dried overnight in the sterile biosafety cabinet. Each insert was washed with PBS-/- twice, preceding cell seeding the following day. HUVECs (80 000) were seeded on the collagen-treated inserts and cultured for 3–4 days before use. HUVECs were stained with CellTrace Cell Proliferation Kit (CFSE, Invitrogen Molecular Probes) according to the manufacturer's indications to confirm the confluency of the HUVEC monolayer. Freshly isolated HUVECs between passages P1 to P3 were used for this assay.

Isolated human neutrophils from heparinized blood were obtained following a Histopaque-1119 (Density 1.119 g mL^{-1}, Sigma-Aldrich) and Ficoll-Paque (Density 1.078 g mL^{-1}, Cytiva) gradient. Isolated neutrophils (10^5) in 100 µL of donor-specific heparin plasma were allowed to phagocytose rhodamine B-labeled Poly-SA rods or spheres for 1 h at 37 °C and 5% CO_2. A ratio of particles-to-neutrophils of 16:1 for 2 and 1 µm rods and spheres and 80:1 for 500 nm rods and spheres were used. These particle-to-cell ratios were chosen to maximize phagocytosis. After particle uptake, neutrophils were washed with cell media to remove excess plasma prior to placement on the permeable insert. Particle-treated neutrophils were added to the HUVEC monolayer/insert and allowed to migrate to the lower compartment due to IL-8 chemotaxis (20 ng mL^{-1}, BioLegend). After 1.5 h, the migrated neutrophils were collected from the lower compartment and stained with anti-human CD11b (0.1 µg sample^{-1}, APC/Cy7, BioLegend) for cell counting using flow cytometry.

Neutrophil transmigration assays were repeated but with PLGA spheres and rods. PLGA spheres (2 µm) and 2 µm AR7 rods were used for this assay, and a particle-to-neutrophil ratio of 16:1 was chosen.

Isolated neutrophils were incubated with spheres or rods at the specified particle-to-cell ratios to determine the extent of phagocytosis and neutrophil viability after particle uptake. Samples were stained with anti-human CD11b (0.1 µg sample^{-1}, APC/Cy7, BioLegend) and Fixable Viability Dye (eFluor 450, eBioscience). Particle-positive and viable neutrophils were established using flow cytometry.

F-Actin Measurements of IL-8-Activated Particle-Treated Neutrophils: Isolated neutrophils in donor-specific heparin plasma (10^6 mL^{-1}) were pre-incubated for 1 h with rhodamine-labeled Poly-SA spheres or AR6 rods at 37 °C and 5% CO_2 as described above. Particle-treated neutrophils were incubated with or without IL-8 (20 ng mL^{-1}, BioLegend) for 60 s. Neutrophils were immediately fixed, permeabilized, and stained for F-actin using the IntraPrep kit (Beckman Coulter) following the manufacturer's instructions. Briefly, unstimulated neutrophils or neutrophils activated with IL-8 were fixed with Fixation Reagent 1 (Formaldehyde) for 15 min on ice. Next, neutrophils were washed in FACS buffer at 500 rcf for 5 min, followed by a 30-minute incubation on ice with ActinGreen 488 ReadyProbes (F-actin, Thermo Fisher Scientific) diluted 1:1000 in Permeability Reagent 2 (Saponine). Cells were washed twice with FACS buffer at 500 rcf for 5 min and analyzed using flow cytometry. Neutrophils were gated based on their forward and side scatter, and the F-actin content was expressed as the mean fluorescence intensity (MFI) of at least 10 000 cells.

To assess F-actin distribution after IL-8 stimulation, neutrophils were plated on a 0.1% poly-*L*-lysine-coated 96-well glass plate for cell attachment. F-actin distribution on neutrophils was assessed by capturing images of plated cells using a Nikon A1S confocal microscope equipped with a 40× water immersion objective, maintaining the same laser intensity across all samples. Images were taken every 0.5 µm (z-height), and the images shown in the manuscript represent the middle section.

Confocal Microscopy of Particle-Treated Neutrophils: Neutrophils were isolated from whole blood and treated with rhodamine-B-labeled Poly-SA spheres and AR6 rods as described above. To confirm particle internalization, the cell membrane of isolated neutrophils was stained with wheat germ agglutinin (Alexa Fluor 488, 2 µg mL^{-1}, Fisher Scientific) and plated on a 0.1% poly-*L*-lysine-coated 96-well glass plate for cell stabilization. Particle per cell count was determined by taking images of plated cells with a Nikon A1S confocal microscope with a 40× water immersion objective.

ELISAS: IgM, TNF-α, and IL-6 ELISAS were purchased from Invitrogen, and MIP-2 and KC ELISAS were purchased from PeproTech (Fisher Scientific). All ELISAS were done according to manufacturing instructions to quantify the protein and cytokine content of the BALF samples collected in the ALI mouse model.

Histology: Mouse lung (left lobe) and liver (left lobe) were collected after LPS instillation and particle treatment. Samples were paraffin-embedded and stained with anti-mouse Ly6G (Cy3) and DAPI for immunofluorescence imaging. The Molecular Pathology Research Laboratory at the University of Michigan paraffin-embedded, sectioned, stained, and imaged the samples.

Statistics: Unless stated otherwise, each graph represents data plotted with average and standard error bars. In experiments involving human blood, each data point (represented by a circle) indicated the average of at least two replicates from independent blood donors within each experimental group. In experiments involving mouse blood, pooled blood from at least five mice was collected, and each data point (represented by a circle) corresponded to a replicate from each experimental group. In particle degradation experiments, data represented the average of at least two replicates per experimental group. Statistical analysis of data was performed using GraphPad Prism. A two-tailed unpaired or paired Student's *t*-test, along with one-way ANOVA or one-way repeated measure ANOVA followed by Fisher's LSD or Tukey's post-test, was used to determine statistical significance between experimental groups.

Supporting Information

Supporting Information is available from the Wiley Online Library or from the author.

Acknowledgements

This work was funded by the National Science Foundation Graduate Research Fellowship (M.V.G. and E.R.B.), the University of Michigan Rackham Merit Fellowship (M.V.G.), and NIH T32 (T32GM145304) (M.L.F.). Additionally, this work was funded by NIH R01 HL145709 (O.E.-A.). The Molecular Pathology Research Laboratory performed histological work funded by NIH P30 CA04659229.

Conflict of Interest

O.E.-A filed a U.S. patent titled "Polymer Particles for Neutrophil Injury" (U.S. Application No: US20240197638A1). The other authors declare no other competing interests.

Author Contributions

M.V.G. and O.E.-A. designed experiments and drafted the manuscript. M.V.G. analyzed and interpreted data. M.V.G., E.R.B, L.D.P., D.K., and M.L.F. performed experiments. M.R.N.L. and K.E.U. fabricated Poly-SA polymers and reviewed the data.

Data Availability Statement

The data presented in this work are available upon request and provided by the corresponding author.

Keywords

acute inflammation, neutrophil intervention, neutrophil transmigration, phagocytosis, rod-shaped particles

Received: December 9, 2024
Revised: April 25, 2025
Published online: May 9, 2025

[1] T. Németh, M. Sperandio, A. Mócsai, *Nat. Rev. Drug Discovery* **2020**, *19*, 253.
[2] E. R. Brannon, M. V. Guevara, N. J. Pacifici, J. K. Lee, J. S. Lewis, O. Eniola-Adefeso, *Nat. Rev. Mater.* **2022**, *7*, 796.
[3] E. Kolaczkowska, P. Kubes, *Nat. Rev. Immunol.* **2013**, *13*, 159.
[4] B. Gierlikowska, A. Stachura, W. Gierlikowski, U. Demkow, *Front. Pharmacol.* **2021**, *12*, 666732.
[5] G. L. Burn, A. Foti, G. Marsman, D. F. Patel, A. Zychlinsky, *Immunity* **2021**, *54*, 1377.
[6] J. Grommes, O. Soehnlein, *Mol. Med.* **2011**, *17*, 293.
[7] X. Shen, K. Cao, Y. Zhao, J. Du, *Front. Pharmacol.* **2021**, *12*, 644270.
[8] C. Tang, C. Wang, Y. Zhang, L. Xue, Y. Li, C. Ju, C. Zhang, *Nano Lett.* **2019**, *19*, 4470.
[9] T. Lisman, *Cell Tissue Res.* **2018**, *371*, 567.
[10] M. Yao, J. Ma, D. Wu, C. Fang, Z. Wang, T. Guo, J. Mo, *Front. Immunol.* **2023**, *14*, 1198952.
[11] S. Pu, D. Wang, D. Liu, Y. Zhao, D. Qi, J. He, G. Zhou, *BMC Pulm. Med.* **2017**, *17*, 148.
[12] Q. Ding, Y. Wang, C. Yang, D. Tuerxun, X. Yu, *Intensive Care Res.* **2023**, *3*, 140.
[13] T. J. Peck, K. A. Hibbert, *F1000Research* **2019**, *8*, F1000.
[14] Enlimomab Acute Stroke Trial Investigators, *Neurology* **2001**, *57*, 1428.
[15] J. M. Harlan, R. K. Winn, *Crit. Care Med.* **2002**, *30*, S214.
[16] P. Mertens, A. Maes, J. Nuyts, A. Belmans, W. Desmet, E. Esplugas, F. Charlier, J. Figueras, G. Sambuceti, M. Schwaiger, L. Mortelmans, F. Van de Werf, *Am. Heart J.* **2006**, *152*, 125e1.
[17] D. Kupor, M. L. Felder, S. Kodikalla, X. Chu, O. Eniola-Adefeso, *Adv. Drug Delivery Rev.* **2024**, *209*, 115316.
[18] C. A. Fromen, W. J. Kelley, M. B. Fish, R. Adili, J. Noble, M. J. Hoenerhoff, M. Holinstat, O. Eniola-Adefeso, *ACS Nano* **2017**, *11*, 10797.
[19] E. R. Brannon, W. J. Kelley, M. W. Newstead, A. L. Banka, K. E. Uhrich, C. E. O'Connor, T. J. Standiford, O. Eniola-Adefeso, *Adv. Healthcare Mater.* **2021**, *11*, 2101534.
[20] K. Bachmaier, A. Stuart, A. Singh, A. Mukhopadhyay, S. Chakraborty, Z. Hong, L.i Wang, Y. Tsukasaki, M. Maienschein-Cline, B. B. Ganesh, P. Kanteti, J. Rehman, A. B. Malik, *ACS Nano* **2022**, *16*, 4084.
[21] Z. Wang, J. Li, J. Cho, A. B. Malik, *Nat. Nanotechnol.* **2014**, *9*, 204.
[22] A. L. Banka, M. V. Guevara, E. R. Brannon, N. Q. Nguyen, S. Song, G. Cady, D. J. Pinsky, K. E. Uhrich, R. Adili, M. Holinstat, O. Eniola-Adefeso, *Nat. Commun.* **2023**, *14*, 2462.
[23] E. Saito, R. Kuo, R. M. Pearson, N. Gohel, B. Cheung, N. J. C. King, S. D. Miller, L. D. Shea, *J. Controlled Release* **2019**, *300*, 185.
[24] J. W. Myerson, P. N. Patel, K. M. Rubey, M. E. Zamora, M. H. Zaleski, N. Habibi, L. R. Walsh, Y.-W. Lee, D. C. Luther, L. T. Ferguson, O. A. Marcos-Contreras, P. M. Glassman, L. L. Mazaleuskaya, I. Johnston, E. D. Hood, T. Shuvaeva, J. Wu, H.-Y. Zhang, J. V. Gregory, R. Y. Kiseleva, J. Nong, T. Grosser, C. F. Greineder, S. Mitragotri, G. S. Worthen, V. M. Rotello, J. Lahann, V. R. Muzykantov, J. S. Brenner, *Nat. Nanotechnol.* **2021**, *17*, 86.
[25] W. J. Kelley, P. J. Onyskiw, C. A. Fromen, O. Eniola-Adefeso, *ACS Biomater. Sci. Eng.* **2019**, *5*, 6530.
[26] Z. Song, J. Fang, Z. Wang, R. Xiao, X. Guo, S. Zhou, *Adv. Funct. Mater.* **2023**, *33*, 2212326.
[27] H. Safari, W. J. Kelley, E. Saito, N. Kaczorowski, L. Carethers, L. D. Shea, O. Eniola-Adefeso, *Sci. Adv.* **2020**, *6*, aba1474.
[28] R. Delgado-Rivera Rosario-Melendez Roselin, W. Yu, Uhrich, K. E., *J. Biomed. Mater. Res. A.* **2008**, *23*, 1.
[29] R. Rosario-Meléndez, M. A. Ouimet, K. E. Uhrich, *Polym. Bull.* **2013**, *70*, 343.
[30] X.-M. Xu, L. Sansores-Garcia, X.-M. Chen, N. Matijevic-Aleksic, M. Du, K. K. Wu, *Proc. Natl. Acad. Sci. U. S. A.* **1999**, *96*, 5292.
[31] R. Amann, B. A. Peskar, *Eur. J. Pharmacol.* **2002**, *447*, 1.
[32] E. R. Brannon, L. D. Piegols, G. Cady, D. Kupor, X. Chu, M. V. Guevara, M. R. N. Lima, Y. Kanthi, D. J. Pinsky, K. E. Uhrich, et al., *Adv. Healthcare Mater.* **2024**, 2400443.
[33] A. J. Thompson, E. M. Mastria, O. Eniola-Adefeso, *Biomaterials* **2013**, *34*, 5863.
[34] A. Margraf, C. A. Lowell, A. Zarbock, *Blood* **2022**, *139*, 2130.
[35] B. Beck-Schimmer, R. C. Schimmer, R. L. Warner, H. Schmal, G. Nordblom, C. M. Flory, M. E. Lesch, H. P. Friedl, D. J. Schrier, P. A. Ward, *Am. J. Respir. Cell Mol. Biol.* **1997**, *17*, 344.
[36] J. G. Moreland, R. M. Fuhrman, J. A. Pruessner, D. A. Schwartz, *Am. J. Respir. Cell Mol. Biol.* **2002**, *27*, 474.
[37] P. Kolhar, A. C. Anselmo, V. Gupta, K. Pant, B. Prabhakarpandian, E. Ruoslahti, S. Mitragotri, *Proc. Natl. Acad. Sci. U. S. A.* **2013**, *110*, 10753.
[38] K. Namdee, A. J. Thompson, A. Golinski, S. Mocherla, D. Bouis, O. Eniola-Adefeso, *Atherosclerosis* **2014**, *237*, 279.
[39] Y. W. Lim, W. S. Tan, K. L. Ho, A. R. Mariatulqabtiah, N. H. Abu Kasim, N. A. Rahman, T. W. Wong, C. F. Chee, *Pharmaceutics* **2022**, *14*, 614.
[40] R. E. Roberts, M. B. Hallett, *Int. J. Mol. Sci.* **2019**, *20*, 1383.
[41] S. Dewitt, M. Hallett, *J. Leukoc. Biol.* **2007**, *81*, 1160.

[42] T. Coates, R. Watts, R. Hartman, T. Howard, *J. Cell Biol.* **1992**, *117*, 765.
[43] M. Keszei, L. S. Westerberg, *J. Immunol. Res.* **2014**, *2014*, 303782.
[44] M. B. Fish, A. J. Thompson, C. A. Fromen, O. Eniola-Adefeso, *Ind. Eng. Chem. Res.* **2015**, *54*, 4043.
[45] J. A. Champion, S. Mitragotri, *Proc. Natl. Acad. Sci. U. S. A.* **2006**, *103*, 4930.
[46] M. Cooley, A. Sarode, M. Hoore, D. A. Fedosov, S. Mitragotri, A. S. Gupta, *Nanoscale* **2018**, *10*, 15350.
[47] Z. Zhou, X. Ma, E. Jin, J. Tang, M. Sui, Y. Shen, E. A. Van Kirk, W. J. Murdoch, M. Radosz, *Biomaterials* **2013**, *34*, 5722.
[48] Y. Geng, P. Dalhaimer, S. Cai, R. Tsai, M. Tewari, T. Minko, D. E. Discher, *Nat. Nanotechnol.* **2007**, *2*, 249.
[49] L. V. Le, P. Mohindra, Q. Fang, R. E. Sievers, M. A. Mkrtschjan, C. Solis, C. W. Safranek, B. Russell, R. J. Lee, T. A. Desai, *Biomaterials* **2018**, *169*, 11.
[50] J. R. Pinney, K. T. Du, P. Ayala, Q. Fang, R. E. Sievers, P. Chew, L. Delrosario, R. J. Lee, T. A. Desai, *Biomaterials* **2014**, *35*, 8820.
[51] J. Allen, J. Ryu, A. Maggi, B. Flores, J. R. Greer, T. Desai, *Tissue Eng., Part A* **2016**, *22*, 142.
[52] N. Kapate, J. R. Clegg, S. Mitragotri, *Adv. Drug Delivery Rev.* **2021**, *177*, 113807.
[53] P. Decuzzi, B. Godin, T. Tanaka, S. Y. Lee, C. Chiappini, X. Liu, M. Ferrari, *J. Controlled Release* **2010**, *141*, 320.
[54] X. Huang, L. Li, T. Liu, N. Hao, H. Liu, D. Chen, F. Tang, *ACS Nano* **2011**, *5*, 5390.
[55] Arnida, M. M. J.-A., A. Ray, C. M. Peterson, H. Ghandehari, *Eur. J. Pharm. Biopharm.* **2011**, *77*, 417.
[56] S. Yi, S. D. Allen, Y.-G. Liu, B. Z. Ouyang, X. Li, P. Augsornworawat, E. B. Thorp, E. A. Scott, *ACS Nano* **2016**, *10*, 11290.
[57] N. Habibi, T. D. Brown, K. Adu-Berchie, S. Christau, J. E. Raymond, D. J. Mooney, S. Mitragotri, J. Lahann, *Langmuir* **2022**, *38*, 5603.
[58] E. G. G. Sprenkeler, S. S. V. Henriet, A. T. J. Tool, I. C. Kreft, I. van der Bijl, C. E. M. Aarts, M. van Houdt, P. J. J. H. Verkuijlen, K. van Aerde, G. Jaspers, A. van Heijst, W. Koole, T. Gardeitchik, J. Geissler, M. de Boer, S. Tol, C. W. Bruggeman, F. P. J. van Alphen, H. J. M. P. Verhagen, E. van den Akker, H. Janssen, R. van Bruggen, T. K. van den Berg, K. D. Liem, T. W. Kuijpers, *Blood* **2020**, *135*, 2171.
[59] S. H. Zigmond, H. I. Levitsky, B. J. Kreel, *J. Cell Biol.* **1981**, *89*, 585.
[60] L. E. Hind, W. J. B. Vincent, A. Huttenlocher, *Dev. Cell* **2016**, *38*, 161.
[61] E. G. G. Sprenkeler, A. T. J. Tool, S. S. V. Henriet, R. van Bruggen, T. W. Kuijpers, *Blood* **2022**, *139*, 3166.
[62] K. Ley, C. Laudanna, M. I. Cybulsky, S. Nourshargh, *Nat. Rev. Immunol.* **2007**, *7*, 678.
[63] A. Zak, S. Dupré-Crochet, E. Hudik, A. Babataheri, A. I. Barakat, O. Nüsse, J. Husson, *Biophys. J.* **2022**, *121*, 1381.
[64] C. M. Doerschuk, *Microcirculation* **2001**, *8*, 71.
[65] G. S. Worthen, B. Schwab, E. L. Elson, G. P. Downey, *Science* **1989**, *245*, 183.
[66] K. Yoshida, R. Kondo, Q. Wang, C. M. Doerschuk, *Am. J. Respir. Crit. Care Med.* **2006**, *174*, 689.
[67] H. Saito, J. Lai, R. Rogers, C. M. Doerschuk, *Blood* **2002**, *99*, 2207.
[68] P. Baluk, A. Hirata, G. Thurston, T. Fujiwara, C. R. Neal, C. C. Michel, D. M. McDonald, *Am. J. Physiol.: Lung Cell. Mol. Physiol.* **1997**, *272*, L155.
[69] L. Claesson-Welsh, E. Dejana, D. M. Mcdonald, *Trends Mol. Med.* **2021**, *27*, 314.
[70] D. Chu, J. Gao, Z. Wang, *ACS Nano* **2015**, *9*, 11800.
[71] D. Chu, X. Dong, Q. Zhao, J. Gu, Z. Wang, *Adv. Mater.* **2017**, *29*, 1701021.
[72] Z. Luo, Y. Lu, Y. Shi, M. Jiang, X. Shan, X. Li, J. Zhang, B. Qin, X.u Liu, X. Guo, J. Huang, Y.u Liu, S. Wang, Q. Li, L. Luo, J. You, *Nat. Nanotechnol.* **2023**, *18*, 647.